Taylor & Francis
Taylor & Francis Group

Australian Journal of Earth Sciences

An International Geoscience Journal of the Geological Society of Australia

ISSN: 0812-0099 (Print) 1440-0952 (Online) Journal homepage: http://www.tandfonline.com/loi/taje20

Quantitative discrimination of normal fault segment growth and its geological significance: example from the Tanan Depression, Tamtsag Basin, Mongolia

H. X. Wang, X. F. Fu, S. R. Liu, R. Chu, B. Liu & P. P. Shi

To cite this article: H. X. Wang, X. F. Fu, S. R. Liu, R. Chu, B. Liu & P. P. Shi (2018): Quantitative discrimination of normal fault segment growth and its geological significance: example from the Tanan Depression, Tamtsag Basin, Mongolia, Australian Journal of Earth Sciences, DOI: 10.1080/08120099.2018.1462850

To link to this article: https://doi.org/10.1080/08120099.2018.1462850

Published online: 27 Jun 2018.

AUSTRALIAN JOURNAL OF EARTH SCIENCES, 2018
https://doi.org/10.1080/08120099.2018.1462850

Quantitative discrimination of normal fault segment growth and its geological significance: example from the Tanan Depression, Tamtsag Basin, Mongolia

H. X. Wang [a,b,c], X. F. Fu [a,b,c], S. R. Liu [a,b], R. Chu [a,b], B. Liu [a,b] and P. P. Shi [d]

[a]CNPC Fault Controlling Reserviors Laboratory, Northeast Petroleum University, 163318, Daqing Heilongjiang, PR China; [b]Science and Technology Innovation Team in Heilongjiang Province 'Fault Deformation, Sealing and Fluid Migration,' 163318, Daqing Heilongjiang, PR China; [c]The State Key Laboratory Base of Unconventional Oil and Gas Accumulation and Exploitation, Northeast Petroleum University, 163318, Daqing Heilongjiang, PR China; [d]The Bohai Oil Research Institute, Tianjin Branch of CNOOC Limited, 300452, Tianjin, PR China

ABSTRACT

This work focuses on quantitative discrimination of fault segment growth and its effect on sedimentation and stratigraphic evolution in the Tanan Depression, the Tamtsag Basin, Mongolia. Integrated seismic data sets and stratigraphic data suggest that normal faults evolve as fault segments grow, link and amalgamate to form a larger fault. Three main stages in the evolution of fault zone are recorded in the syn-rift stratigraphy. This paper applies a method to effectively discriminate the locus of fault segments by 'three diagrams' and quantitatively reconstruct process of fault growth by the maximum throw subtraction method. Backstripped to T_{23} SB event, the F1 fault comprises four hard-linked segments, and the F2 fault is divided into four soft-linked segments (F2-4 and F2-5 segments are shown by hard linkage) at the T_{23} structural level. The F1 and F2 fault comprise hard-linked segments at the $T_{23\text{-}1}$ structural level when the F1 and the F2 are backstripped to the T_{22} (133.9 Ma) SB event. The F1 fault is divided into three soft-linked segments (F1-2 and F1-3 segments are shown by hard linkage), and the F2 fault is divided into four isolated fault segments at the $T_{23\text{-}1}$ structural level when the F1 and the F2 is backstripped to the T_{23} SB event. Incorporation of paleo-fault geometry, isochron thickness map and sedimentary facies suggest that the transfer zone provided accommodation space for sediment discharge and deposition, and the depocentres were formed at the locus of maximum throw along a fault segment during its overall deposition.

ARTICLE HISTORY
Received 30 October 2017
Accepted 12 March 2018

KEYWORDS
Tamtsag Basin; Tanan Depression; fault segment growth; throw backstripping; transfer zone; sedimentary stratigraphy

Introduction

Throughout decades of hydrocarbon exploration, geologists have realised that faults are important in sediment distribution (e.g. sag structure and sandstone), especially in rift basins. The maximum displacement/length ($d_{\max}/L$) ratio for mature faults range between 10^0 and 10^{-3}, and primarily between -10^{-1} and 10^{-2} (Figure 1) (Schultz & Fossen, 2002), whereas the $d_{\max}/L$ ratio relationship for single-event normal faults or segments ranges between 10^{-3} and 10^{-6}, and primarily between 10^{-5} and 10^{-4} (Wells & Coppersmith, 1994). The displacement is generally less than 10 m for a single-event fault (Figure 1). This suggests that geological faults represent many ($\sim 10^3$) individual slip events (Fu, Xu, Wei, & Lv, 2012; Kim & Sanderson, 2005). Fault growth is the result of progressive fracture deformation (Scholz, Dawers, Yu, Anders, & Cowie, 1993), or is associated with the nucleation, growth and linkage of fault segments during progressive deformation. Four fault growth models were illustrated by Kim and Sanderson (2005). (1) A 'constant d_{max}/L ratio model,' which is generally applied for small, isolated faults. The fault length increases as the displacement increases, and the d_{max}/L ratio is constant throughout the evolution. (2) An 'increasing d_{max}/L ratio model' that presents an increasing d_{max}/L ratio with increasing fault growth. (3) A 'constant length model' suggested by Walsh, Nicol, and Childs (2002), in which the fault length is attained rapidly at an early stage and remains constant as displacement increases. (4) A 'fault linkage model' (e.g. Cartwright, Trudgill, & Mansfield, 1995; Fu, Sun, Wang, & Meng, 2015; Kim, Andrews, & Sanderson, 2000; Kin & Sanderson, 2005; Peacock & Sanderson, 1991), in which the faults grow as isolated faults at early stages and then link together to produce additional fault length. During their growth, fault segments can propagate from multiple initiation points to form relay ramps and subsequently link together to constitute a single coalesced corrugated fault surface (Fu et al., 2012; Gupta & Scholz, 2000; Mansfield & Cartwright, 1996; Peacock & Sanderson, 1991; Soliva & Benedicto, 2004).

Normal faults mostly comprise fault segments that commonly occur as arrays of overlapping segments (Anders & Schlische, 1994; Childs et al., 2009; Fossen, 2010; Kim &

CONTACT X. F. Fu fuxiaofei2008@sohu.com
Editorial handling: Keyu Liu

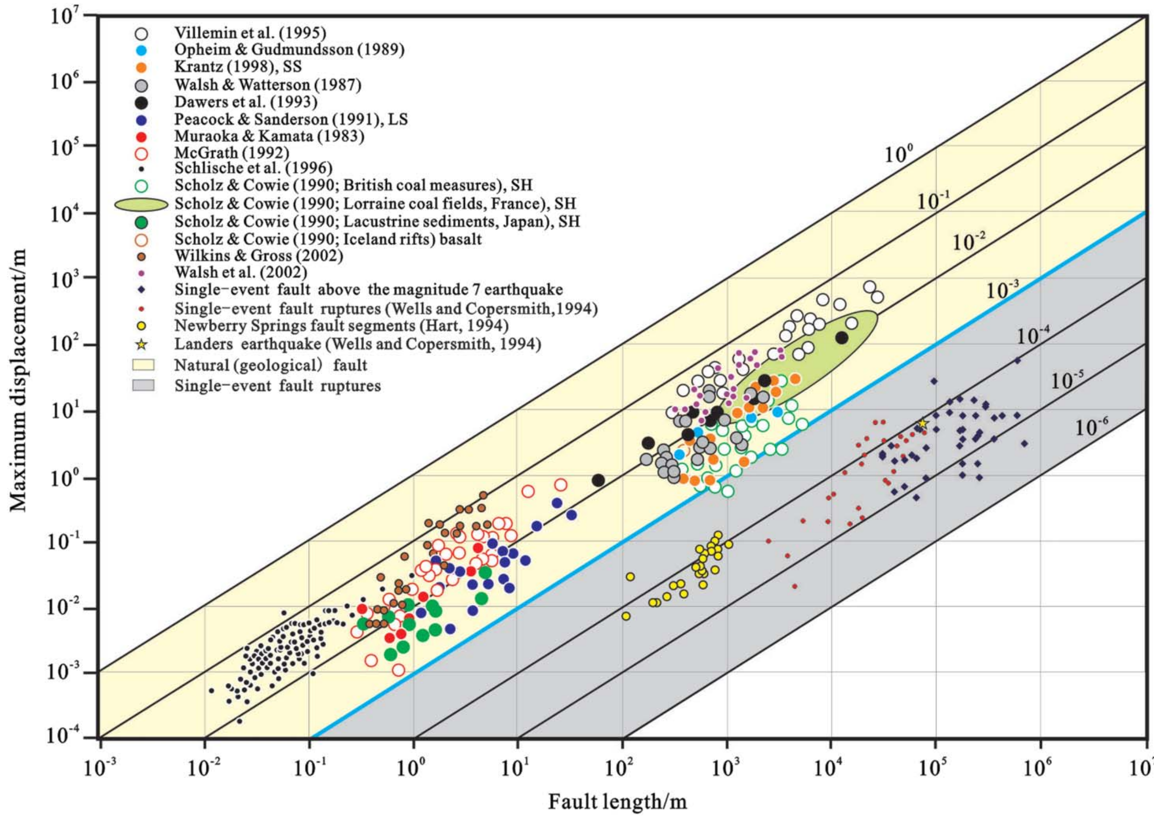

Figure 1. T plots of maximum displacement (d_{max}) against fault length (L) for natural faults and single-event faults. The data for the natural faults are from Kim and Sanderson (2005). Yellow shadow is the natural fault, grey shadow is the single-event fault rupture. SS, sandstone; LS, limestone; SH, shale.

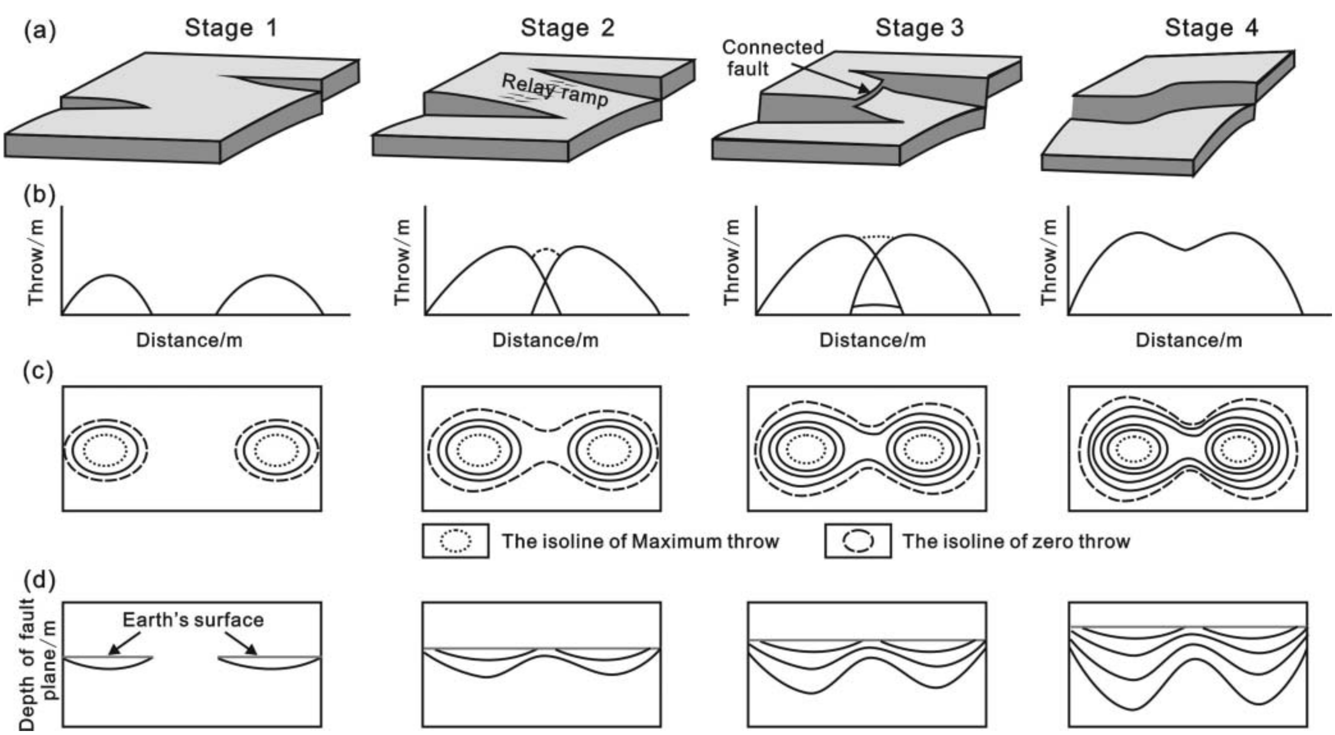

Figure 2. Evolution and quantitative discrimination of fault segment growth. (a) The 3D schematic diagram of the evolution processes of fault segments (Conneally et al., 2014, modified). (b) Throw–distance curve at the stage of fault growth. (c) Fault-plane throw diagram at the stage of fault growth. (d) Fault-plane depth diagram at the stage of fault growth (Fu et al., 2015). Stage 1, isolated fault (approaching transfer zone); Stage 2, soft linkage (overlapping transfer zone); Stage 3, hard linkage (transfer fault); and Stage 4, through-going fault (fault damage zone).

Sanderson, 2005; Segall & Pollard, 1980). It is well understood that normal faults evolve as fault segments, grow, link and amalgamate to form a larger fault (Figure 2). Segment linkage has been proposed as an important mechanism for fault growth at various scales in rift zones (Cartwright et al., 1995; Fu et al., 2015; Kim et al., 2000; Peacock, 1991; Peacock & Sanderson, 1991; Soliva & Benedicto, 2004; Willemse, Pollard, & Aydin, 1996) with the process of fault segment growth well validated by field outcrops, sandstone physical modelling and 3D seismic interpretation (Fossen, 2010; Fu et al., 2015; Kristensen, Childs, & Korstgård, 2008; Wang et al., 2013). Three stages identified in the growth of linked fault segments (Peacock & Sanderson, 1991, 1994) describe the formation of different types of transfer zones as the fault segments grow. Initially, isolated faults (stage 1) can propagate towards each other, leading to an approaching transfer zone (Figure 2a). Fault tips gradually converge and interact. The fault segments may interact without any obvious connection (soft linkage—stage 2) and form a synthetic overlapping transfer zone (Wang et al., 2013) (Figure 2a), with stress focus on the fault bridge (overlapping zone). As faults continue to slip, the fault segments may evolve and link by breaching the relay zone (hard linkage—stage 3), leading to the formation of a through-going fault (Conneally, Childs, & Walsh, 2014; Fu et al., 2015) (Figure 2a).

Segments are, however, transient features in the evolution of a rift zone, as they grow and interact, they may link to form larger structures (Dawers & Anders, 1995; Kim & Sanderson, 2005; Pollard & Aydin, 1988). Therefore, the process of interaction is a necessary step in the evolution of a rift zone over a range of scales. The main basin geometries of rift systems (half-graben or graben) are controlled by major faults (Morley, 1995), with fault segment growth linkages controlling the evolution of depocentres (half-graben or graben) (Dawers & Underhill, 2000). Transfer zones are associated with such faults as transfer zones link major boundary faults that are located on opposite sides of rifts (Gawthorpe & Hurst, 1993) and can therefore cause variations in rift segment geometry (Morley, Nelson, Patton, & Mun, 1990; Rosendahl et al., 1986). As well as on basin formation and depositional patterns (Athmer & Luthi, 2011; Gawthorpe & Hurst, 1993; Morley, 1999, 2002), transfer zones also have considerable influence on hydrocarbon migration and trapping in rift systems (Coskun, 1997; Morley et al., 1990; Peacock & Sanderson, 1994).

This study investigates the linkage process of fault through time and provides insights into the evolution of border fault systems in rifts. This study revealed the history of border fault systems by the maximum throw subtraction method (Dutton & Trudgill, 2009; Rowan, Hart, Nelson, Flemings, & Trudgill, 1998) in the Tanan Depression of the Tamtsag Basin and provides insights into the relationship between sag structure, drainage (sedimentary deposits) development and the border fault system.

Geological background

The Tamtsag Basin, covering an area of ~35 400 km^2 in eastern Mongolia, is part of the Hailar-Tamtsag Basin, which stretches across China and Mongolia (Figure 3) (Ji, Cao, Meng, Zhang, & Qu, 2009). The Hailar-Tamtsag Basin is a widespread intra-continental rift system that formed during Late Jurassic and Cretaceous (Fu, Chen, Yan, Yang, & Sun, 2013; Graham et al., 2001; Meng, Hu, Jin, Zhang, & Xu, 2003; Traynor & Sladen, 1995; Zhou, Ji, Pigott, Meng, & Wan, 2014) and extends up to 300 km long and 80 km wide, covering an area of 79 610 km^2 (Figure 3a). The Tamtsag Basin is a SW–NE-trending fault-controlled structure. The Tanan sub-basin, covering an area of 3500 km^2 located in the southern part of the Tamtsag Basin, is NE-trending and fault-controlled with first-order half grabens, bounded by deep seated faults. The Tanan sub-basin can be further subdivided into seven tectonic units, i.e. the eastern fault scarp slope, the eastern half-graben, the central-uplifted high, the central half-graben, the western step-fault, the western half-graben and the western dip slope (Figure 3b) (Fu et al., 2013; Ji et al., 2009; Zhou et al., 2014).

The Tanan Depression is filled with Lower Cretaceous continental sedimentary rocks that can reach up to 4 km in thickness. The succession includes four formations from the base: Tongbomiao Formation (K_1t, 145–139.4 Ma), Nantun Formation (K_1n, 139.4–133.9 Ma), Damoguaihe Formation (K_1d, 133.9–130.8 Ma), and Yimin Formation (K_1y, 130.8–100.5 Ma) (Figure 4). The Tongbomiao Formation is mainly composed of fan-deltaic variegated conglomerate and grey pebbly coarse sandstone, interbedded with shallow lacustrine grey-white mudstone. The Nantun Formation is composed of deep lacustrine dark mudstone, and turbiditic conglomeratic sandstone and sandstone. The Damoguaihe Formation consists mainly of braided-deltaic siltstone to fine-grained sandstone, interbedded with grey laminated mudstone with a gradually upward-shoaling character. The Yimin Formation is composed of fluvial–deltaic fine sandstone and siltstone, interbedded with shallow lacustrine grey mudstones (Figure 4). In the Tamtsag rift basin, the Late Jurassic to Early Cretaceous rift episode consists of three distinct rift phases: pre-rift, syn-rift and post-rift phases (Figure 4). Owing to the varying rate of rifting, the syn-rift phase can be further subdivided into three stages: early syn-rift, rift climax and late syn-rift stages (Jia et al., 2014; Zhou et al., 2014).

The Tanan Depression is an important hydrocarbon-bearing area in Tamtsag Basin (Fu et al., 2013; Zhou et al., 2014). Current knowledge indicates that clastic sediments of the Nantun and Tongbomiao formations contain both excellent source rocks and good reservoir rocks for oil (Fu et al., 2013; Huang et al., 2012; Jia et al., 2014; Miao et al., 2011, 2012). The proven reserves are 120.13 million tons with cumulative production capacity of 5.6 $\times$ 10^5 tons (Wang, 2011). The reserves account for 72.5% of the total reserves, and the hydrocarbons mainly come from the source rocks of middle part of Nantun I member. The hydrocarbon-bearing system developed in the syn-rift climax stage is characterised by 'source rock controlling' or 'sag controlling hydrocarbon' (Hu, 1982; Zhao, Jin, Wang, Han, & Kang, 2011).

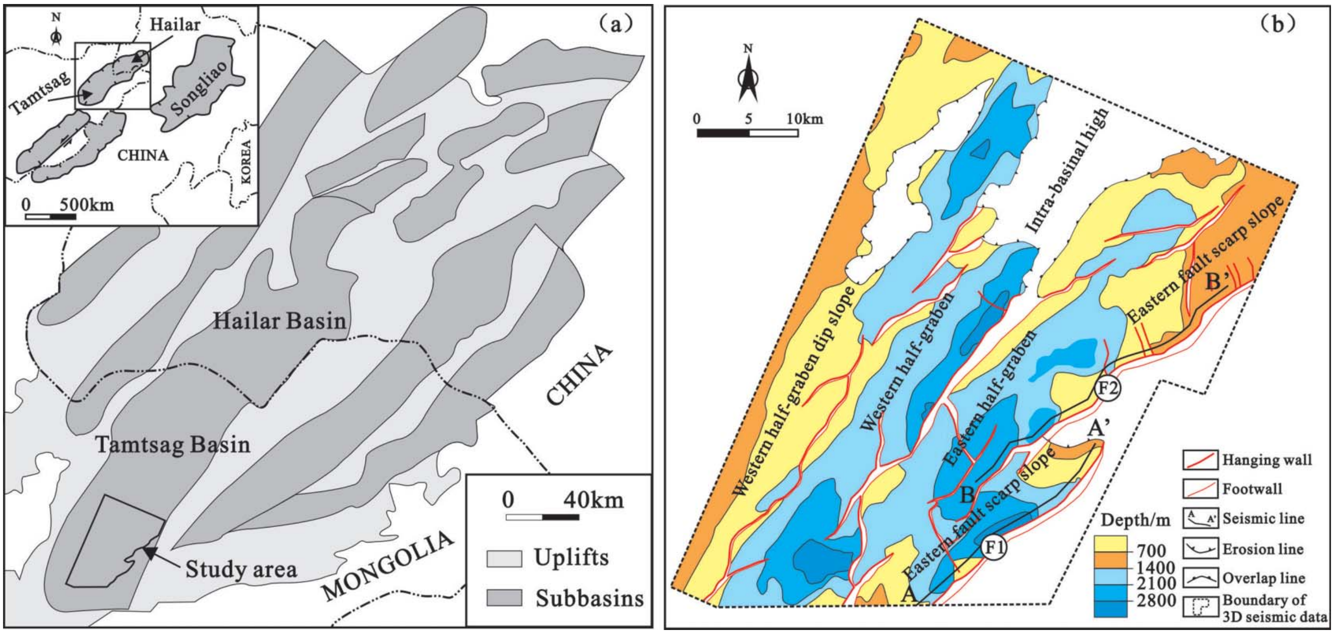

Figure 3. (a) Location and tectonic units of the Tamtsag-Hailar Basin and (b) structural contour map of the T3 seismic reflector (corresponding with the basal Nantun Formation) in the Tanan Depression of the Tamtsag-Hailar Basin (modified from Zhou et al., 2014). F1 and F2, basin boundary faults in the basin. Solid lines (A–A' to B–B") represent the locations of well-seismic correlation sections in the text.

Methodology

Field studies (Soliva & Benedicto, 2004), and physical and numerical modelling (Scholz et al., 1993), suggest that fault growth is a dynamic process (Cartwright et al., 1995; Cartwright, Mansfield, & Trudgill, 1996; Dawers & Anders, 1995; Peacock & Sanderson, 1991; Trudgill & Cartwright, 1994). A geological fault represents many ($\sim 10^3$) individual slip events (Fu et al., 2012; Kim & Sanderson, 2005). Fault segment (en echelon arrangement of normal fault segments) growth is a very common phenomenon, which is one of most important mechanism for fault growth and linkage.

Three stages can be identified in the growth of linked fault segments (Peacock & Sanderson, 1991; Wang et al., 2014): initial isolated faults (stage 1), soft linkage (stage 2), and hard linkage (stage 3). At present, there are thee methods to effectively discriminate the process of fault segments linkage: throw–distance (*T*–*L*) curve (Muraoka & Kamata, 1983; Peacock & Sanderson, 1994; Soliva & Benedicto, 2004), fault-plane throw diagram (Morley & Wongana, 2000; Muraoka & Kamata, 1983), and fault-plane depth diagram (Morley, 1999, 2002; Peacock & Sanderson, 1994) (Figure 2).

Discrimination of fault segments

The displacement–distance curve represents the displacement (*D*) of a bedding plane along the traces of the faults (*L*) with a typical isolated fault exhibiting nearly symmetric displacement distribution (Gupta & Scholz, 2000). It has been widely recognised that fault displacement varies within the fault surface, displacement is zero at the fault tips and generally increases to a maximum near the centre of the fault surface (Barnett, Mortimer, Rippon, Walsh, & Watterson, 1987). The typical displacement profile of isolated faults will also be used in both fault sets as a reference to quantify and interpret the evolution of displacement distribution of segmented faults. If the displacements of two overstepping segments were added, there is commonly a minimum in the total fault displacement at the overstep zone. Displacement maxima and minima have been used to infer the centres and tips of individual fault strands that have linked to form a single through-going fault segment (Anders & Schlische, 1994; Peacock & Sanderson, 1991; Young, Gawthorpe, & Sharp, 2002). The displacement–distance profiles for multi-segmented faults may show displacement minima at segment offsets (Kim & Sanderson, 2005; Peacock & Sanderson, 1991; Pei, Paton, Knipe, & Wu, 2017), but linkage points are not always preserved as displacement minima. Throw is the vertical component of the fault displacement. There is a linear relationship between displacement and throw, so we can use 'throw (*T*)' instead of 'displacement' (Figure 2b).

Fault-plane throw diagrams record horizon offsets (i.e. hanging wall and footwall horizon cutoffs) for the special mapped horizons and allow the two-dimensional (2-D) spatial variation of throw on a fault surface to be represented (Morley & Wongana, 2000). Observation of more subtle throw variations may be masked or overlooked by analysis of fault-plane projection diagrams. Throw values along the fault plane typically decrease significantly towards the linkage point, and therefore the minima throw are considered to represent the partitioning or transfer of throw in fault-plane throw diagrams (Figure 2c).

Fault-plane depth diagrams, which record the depth of hanging wall horizon cutoff line for the special horizons, are similar to the seismic section along the fault strike. Owing to the differential subsidence, depths along the fault plane

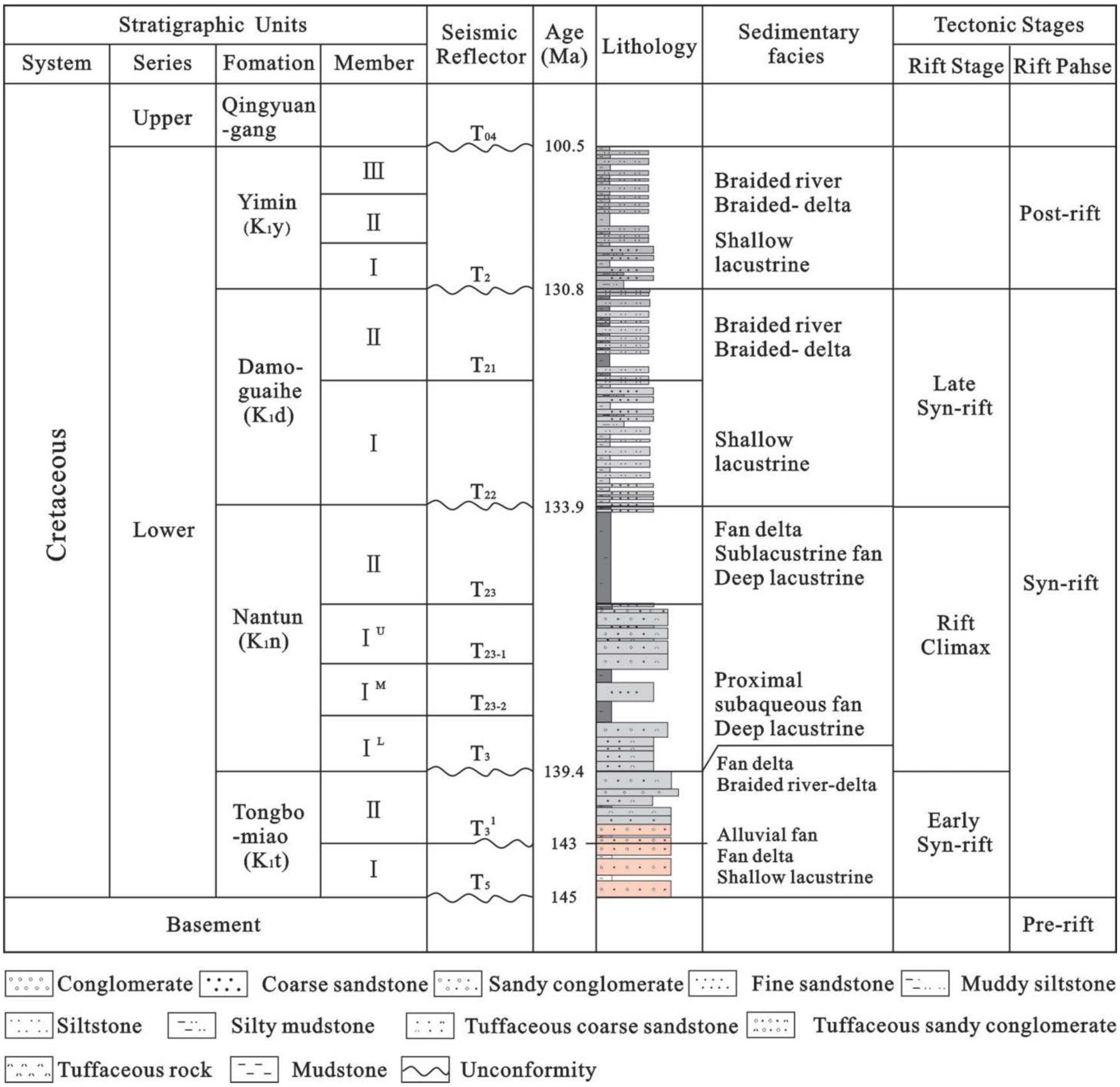

Figure 4. Generalised stratigraphic column of the Lower Cretaceous strata of the Tanan Depression, Tamtsag Basin (modified from Jia et al., 2014; Zhou et al., 2014).

typically shallow towards the linkage dots and deepen away from the linkage point, leading to the formation of transverse folds (Fu et al., 2015; Jackson, Gawthorpe, & Shapp, 2002; Schlische, 1995). Fault strand boundaries commonly represent regions of displacement minima (Gawthorpe & Hurst, 1993; Gawthorpe, Fraser, & Collier, 1994; Schlische, 1995; Schlische, Young, Ackermann, & Gupta, 1996). The transverse fold enables us to determine the location where fault strands have linked together (Figure 2d).

Quantitative discrimination of fault growth stage

Fault growth is a kinematic process. To reconstruct the evolution of the fault and test our proposed interpretations of fault evolution from isochron and present-day geometric analysis, throw backstripping techniques were used. Two different techniques have been applied (Dutton & Trudgill, 2009).

Original method or vertical subtraction method (Figure 5a–c)

The throw pattern at the time of deposition of some horizon is determined at any given location along the length of the fault by subtracting the throw at that horizon from the throw values of deeper horizons below the selected location (Chapman & Meneilly, 1991; Childs et al., 1993). Rowan et al. (1998) argued that, for an elliptical fault shape, the result of this method is that the length of a fault at any level does not change as increments of throw are removed (Figure 5). This means that fault lengths do not grow with time as throw increases and applies to a 'constant length model' that is usually applied for small, isolated faults (Kim & Sanderson, 2005; Walsh et al., 2002) but is a very rare situation.

Maximum throw subtraction method (T_{max}) (Figure 5d–f)

This is a modified technique in which the throw pattern at the time of deposition of some horizon is calculated by

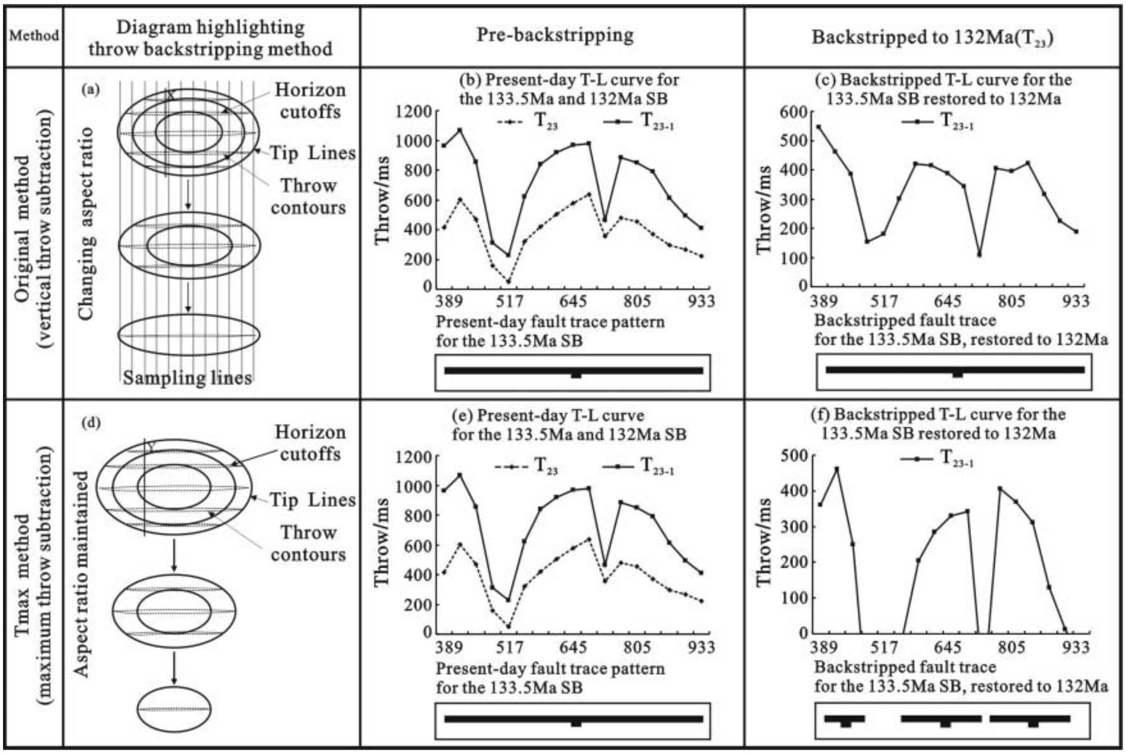

Figure 5. Diagram highlighting two throw backstripping methods (modified from Dutton & Trudgill, 2009; Rowan et al., 1998). (a) Original method or vertical subtraction method. (b) Original method involving subtraction of the uppermost *T–L* profile (132.0 Ma SB) from the underlying *T–L* profile (135.0 Ma SB) resulting in the generation of a reconstructed *T–L* profile (c) On the 135.0 Ma SB event, back to 132.0 Ma. Note the resulting anomalous fault length. (d) Maximum throw subtraction method (T_{max} method). (e) The T_{max} method: the maximum value of throw at the 132.0 Ma SB event is subtracted from each fault segment *T–L* profile at the 135 Ma SB event, backstripping both the throw and lateral tip positions of the fault segments (f). Note the fault length decreases using the T_{max} method. SB, sequence boundary.

subtracting the maximum throw along the horizon from the entire fault surface, resulting in a decrease in fault length as throw is removed (Rowan et al., 1998). Based on the data of maximum displacements and length on faults from earthquake rupture data and published papers, it is generally assumed that there is linear relationship between the maximum cumulative displacement on a fault (d_{max}) and the fault surface (*L*) in logarithmic coordinates (Cowie & Scholz, 1992; Kim & Sanderson, 2005; Watterson, 1986) (Figure 1). For a linear scaling, fault length increases as throw accumulates (Walsh & Watterson, 1988; Watterson, 1986). This method results in a decrease in fault length as throw is removed and therefore provides results that are considered more realistic (Dutton & Trudgill, 2009; Rowan et al., 1998). Note the fault trace length is maintained using the original method but reduces using the T_{max} method.

Quantitative reconstruction of fault segment growth process

At the rifting climax during the deposition of the Nantun Formation, there are two boundary faults, F1 and F2, in the Tanan Depression. 'Three diagrams' of F1 and F2 comprise fault segments (Figures 6 and 7), that grow and interact and may link to form the larger fault. Approximate values of displacement are obtained by measuring the vertical component of the total displacement vector (throw) of strata in milliseconds TWT. Throw is measured on every 16th line in the 3D seismic data set, which was oriented southeast to northwest. The seismic data have not been depth converted; therefore, true displacement cannot be measured accurately, and throw is used as proxy for displacement.

The 'three diagrams' of this area suggest that the F1 and F2 were divided into many fault segments. F1 is composed of four main hard-linked segments separated by displacement minima: F1-1, F1-2, F1-3 and F1-4 fault segments (black dots in Figure 6). Five main linked fault strands have been identified in the F2: F2-1, F2-2, F2-3, F2-4 and F2-5 fault segments (Figure 7). In addition, Figures 6c and 7c also indicate that the transverse folds are formed at the fault growth point, and the onlap seismic reflectors are observed on the transverse folds.

The T_{max} subtraction method (Figure 5d–f) requires the calculation of the maximum throw value at a certain horizon for each fault within the system that is being backstripped in the Tanan Depression. A more regional approach that incorporates backstripping throw from a larger part of the fault down to the 133.9 Ma SB is shown in Figure 8. Applying these techniques allows reconstruction of the *T–L* profiles for various structural levels at different evolutionary stages. As increments of throw are removed, faults generally become shorter, become segmented or disappear completely.

Present-day *T–L* profiles of the F1 and F2 are shown in Figure 8a and are backstripped to the T_{22} (133.9 Ma) and T_{23} SB event in Figure 8 (b, c). Figure 8a shows that the F1 and F2

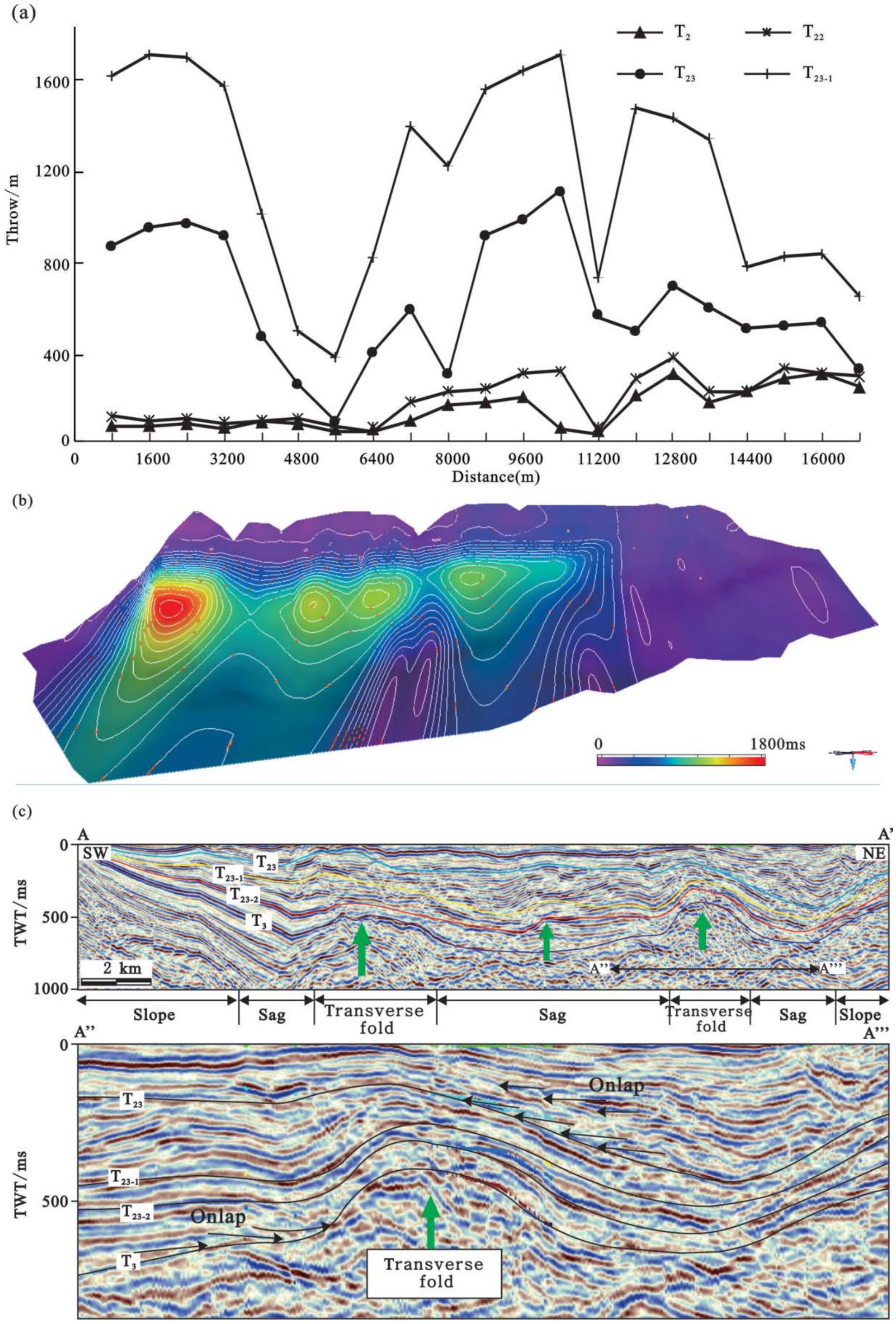

Figure 6. Three diagrams of F1 in the Tanan Depression. (a) Throw–distance curve; throw in metres. (b) Fault-plane throw diagram illustrating the locus of fault segments linkage. (c) Typical seismic cross-section (along the F1 fault strike) (seismic section marked in Figure 3, line A–A'). TWT, two way travel; T_{23}–T_3, seismic reflectors. Black arrows represent the onlaps. Green arrows represent the locations of transverse folds.

are characterised by soft linkage (relay zone) at different structural levels. The principal observation is that the F1 comprises four hard-linked segments, and the F2 is divided into four soft-linked segments (F2-4 and F2-5 segments are shown by hard linkage) at the T_{23} structural level. The F1 and F2 comprise hard-linked segments at the $T_{23\text{-}1}$ structural level when the F1 and F2 are backstripped to T_{22} (133.9 Ma) SB event (Figure 8b).

The F1 is divided into three soft-linked segments (F1-2 and F1-3 segments are shown by hard linkage), and the F2 is

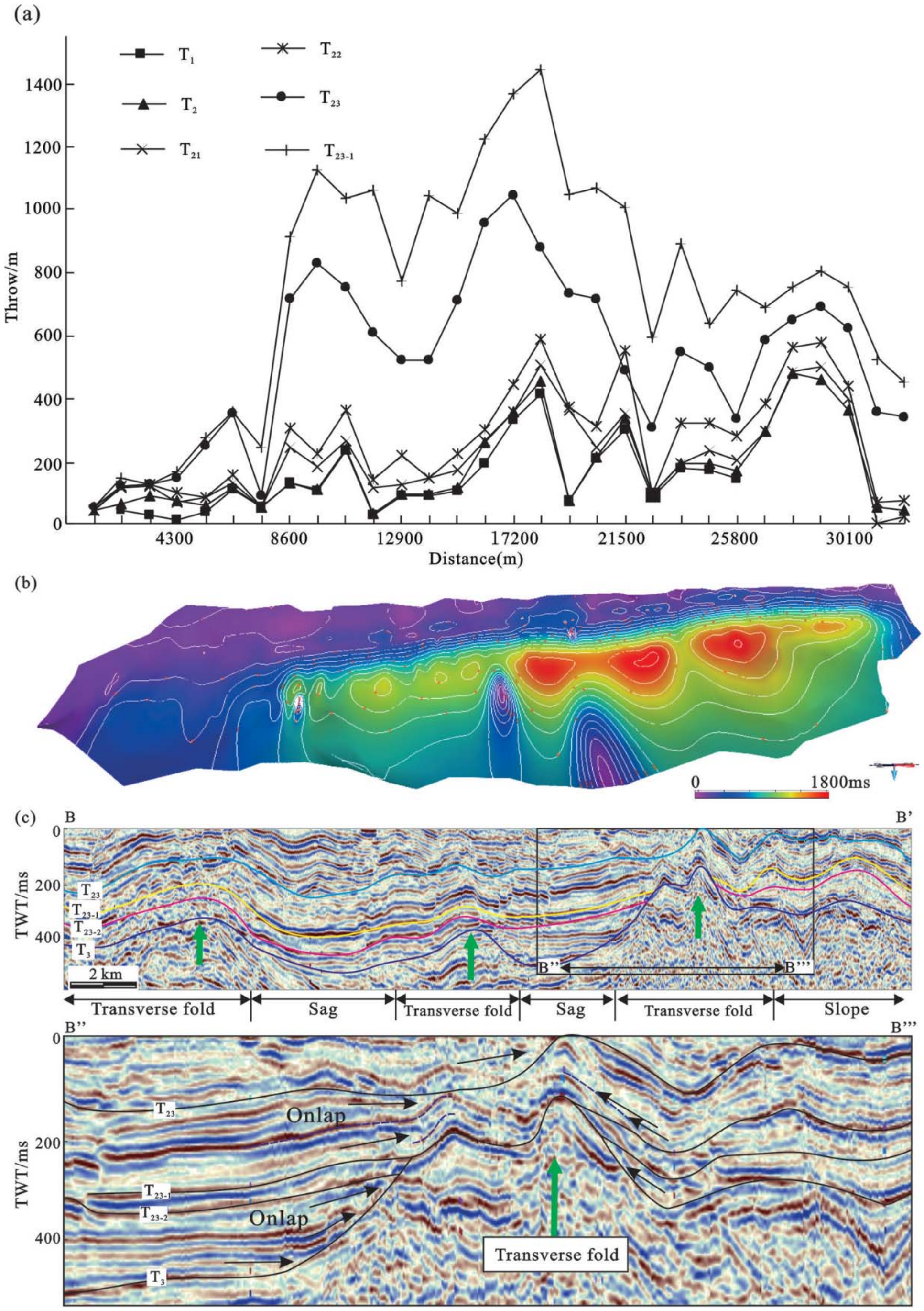

Figure 7. Three diagrams of F2 in the Tanan Depression. (a) Throw–distance curve; throw in metres. (b) Fault-plane throw diagram illustrating the locus of fault segments linkage. (c) Typical seismic cross-section (along the F2 fault strike) (seismic section marked in Figure 3, line B–B'). TWT, two way travel; T_{23}–T_3, seismic reflectors. Black arrows represent the onlaps. Green arrows represent the locations of transverse folds.

divided into four isolated fault segments at the $T_{23\text{-}1}$ structural level when the F1 and F2 are backstripped to T_{23} SB event (Figure 8c).

Implication on timing of fault segment growth and linkage

The temporal and spatial evolution of major normal fault zones is accompanied by changes in basin topography and the location and generation of accommodation zones (Schlische et al., 1996; Young et al., 2002). Therefore, the architecture and distribution of the coeval stratigraphy may potentially provide insights into understanding the tectonic evolution, e.g. the timing of fault segment growth and linkage, which involved two aspects of significance: (1) the fault segment growth and depocentres evolution and (2) the relationship between structural transfer zone and spatial distribution of sandstone.

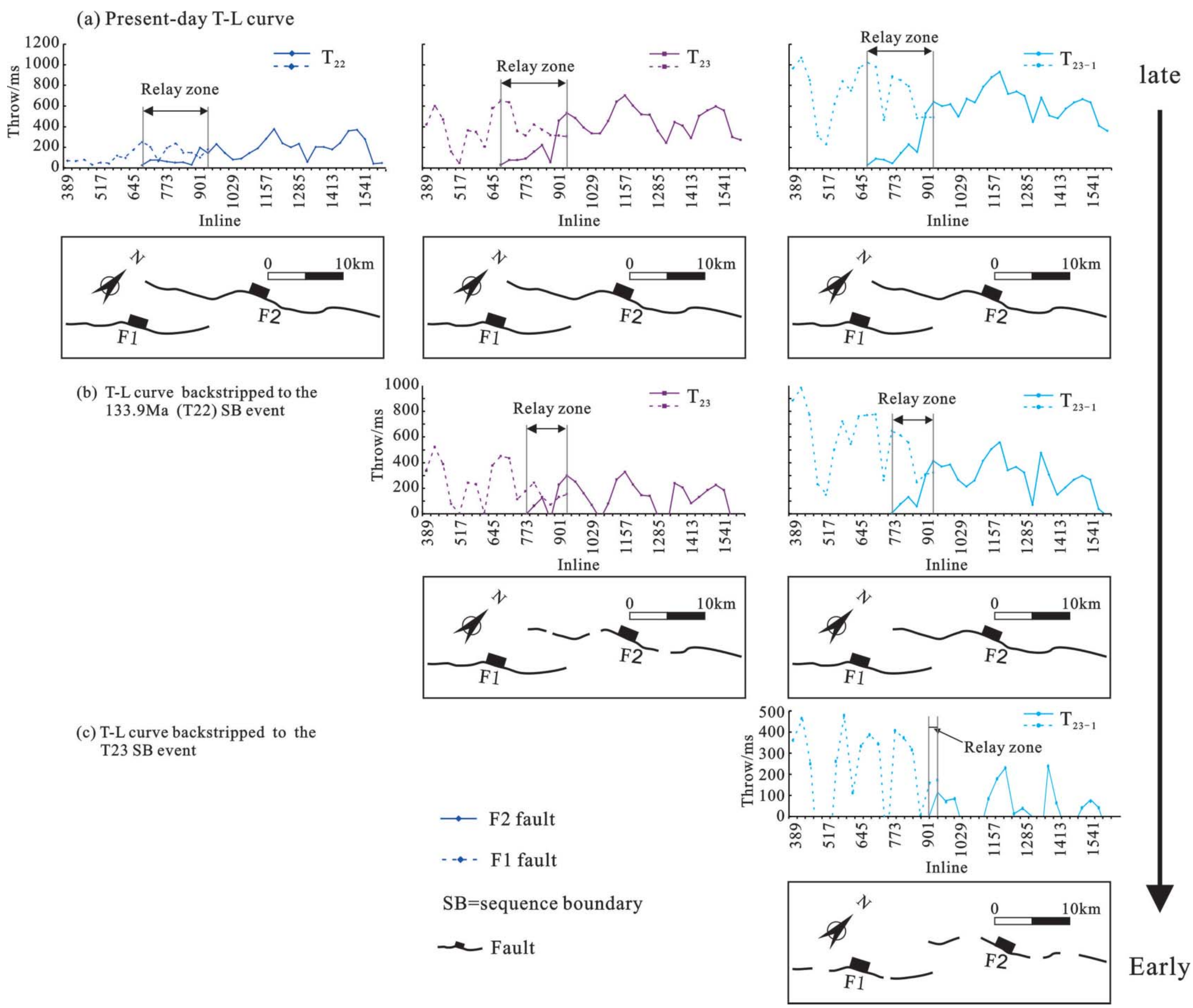

Figure 8. Regional throw-backstripping of a larger part of the F1 and F2 segments in the eastern Tanan. (a) Present-day *T–L* profiles of the F1 and F2 at the T_{22}, T_{23} and $T_{23\text{-}1}$ structural level. (b) Backstripped *T–L* profiles to T_{22} (133.9 Ma) SB event at the T_{23} and $T_{23\text{-}1}$ structural level. (c) Backstripped *T–L* profiles to T_{23} SB event at the $T_{23\text{-}1}$ structural level.

Characteristics of different seismic units based on thickness data and onlap

In the Tanan Depression, the sags are controlled by F1 and F2, which separated by the relay ramp. Integrating the thickness data of seismic units, the seismic section along the fault strike and the seismic reflection character (Figures 5, 6 and 9), suggests a model of sedimentary basin fill with gradual propagation and linkage of the two boundary faults. Thickness (isochron) maps, were generated for the two main seismic divisions (seismic units 1 and 2) of the Upper Cretaceous synrift, which correspond to the upper parts of Nantun Formation members I and II (Figure 10a, b). We have employed a pragmatic approach preserving sediment thickness as a first-order proxy for subsidence (Young et al., 2002).

During the deposition of the Nantun I member (seismic unit 1), seven fault segments are observed (labelled F1-1, F1-2, F1-3 and F2-1, F2-2, F2-3, F2-4), forming seven main isochron thicks (i.e. regions of maximum thickness in ms TWT, labelled D1–D7, Figure 9a), that trend parallel to the faults and are separated by thinner regions. Thickness D1–D6 all occur adjacent to the fault trace, whereas D7 is situated up to about 6 km away from the F1 and thins towards the fault (Figure 9a). Isochron thicks are controlled by seven fault segments and are significantly thinner in the relay zone than in the hanging wall of the fault segments. The thickness gradually decrease towards the tip of fault segments (Figure 9a). On strike-parallel seismic sections within the hanging wall of the F1 and F2, five transverse folds (anticlines) can be identified (labelled H1–H5; Figures 6c and

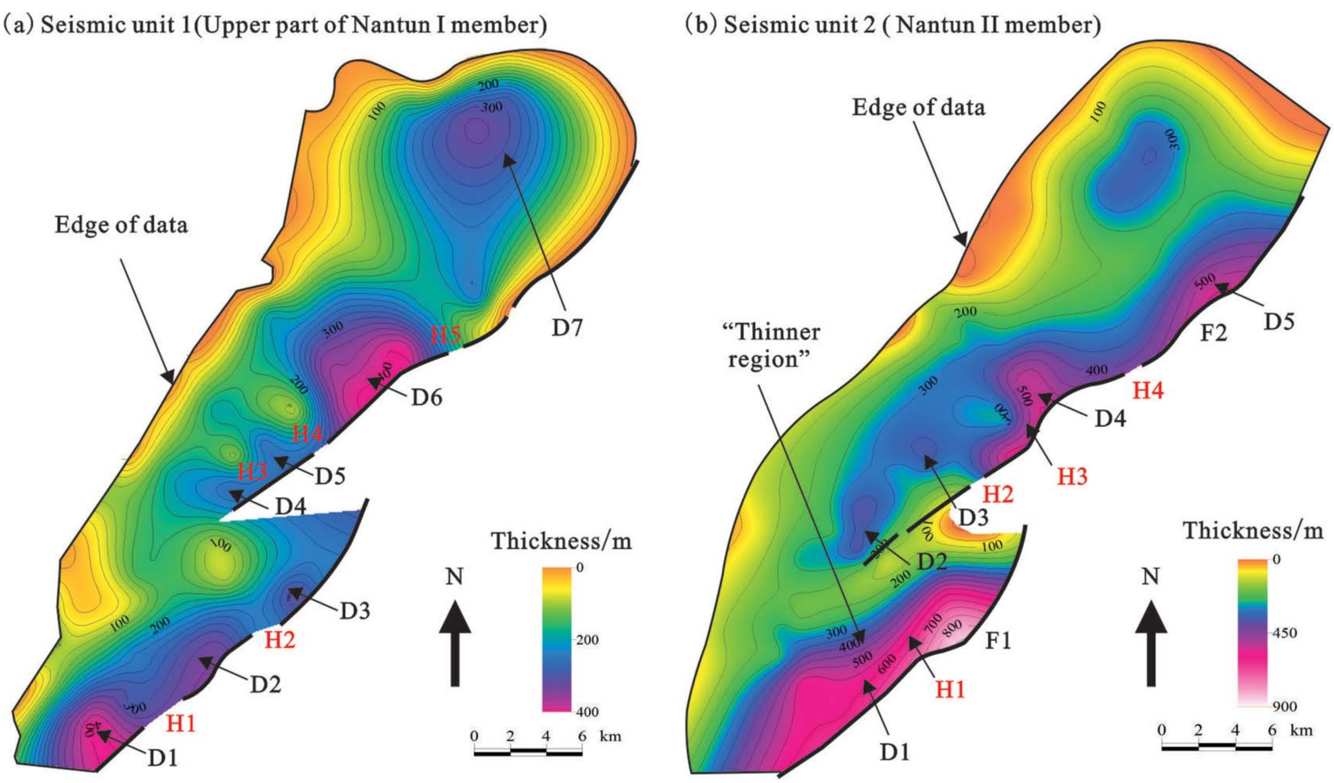

Figure 9. Isochron maps in the eastern fault scarp slope of the Tanan Depression. Solid fault traces indicate a surface breaking fault. H1–H5 refers to the location of transverse fold observed on fault parallel seismic lines (Figures 6c and 7c). (a) Seismic Unit 1, corresponding to upper part of Nantun I member; D1–D7 refer to the major depocentres; F1-1–F1-7 refer to the main fault segment (thick black lines) controlling the location of the depocentres. (b) Seismic Unit 2, corresponding to Nantun II member; D1–D5 refer to the major depocentres.

7c). There are two anticlines in the hanging wall of the F1 and three anticlines in the hanging wall of the F2. The seismic reflectors onlap onto the anticlines (Figures 6c and 7c).

During the deposition of the Nantun II member (seismic unit 2), three fault segments are observed, and three main isochron thicks can be observed in the hanging wall of the F1 and F2 (D1–D5, Figure 9b). Thickness D1, D4 and D5 occur adjacent to the fault trace, whereas D2 and D3 are situated up to about 1–4 km away from the F2 and thin towards the fault (Figure 9b). In the hanging wall of F1, one major isochron thick (D1), with a maximum thickness of 800 m, is evident. The thickness of D1 is greatest in the northeast with two local maximum depocentres separated by a thinner region (H_A) (Figure 9b). In the hanging wall of F2, four major isochron thicks (D2, D3, D4 and D5) are evident with maximum thicknesses of ~400 m, 400 m, 600 m and 600 m, respectively. There are two local maximum depocentres in the D4 area, separated by a thinner region (H3) (Figure 9b). On strike-parallel seismic sections within the hanging wall of the F1 and F2, four transverse folds (anticlines) can be identified (Figures 6c and 7c); one in the hanging wall of the F1, and three in the hanging wall of the F2. The seismic reflectors onlap onto the anticlines in several places (Figures 6c and 7c).

Evolution of F1 and F2 in the Tanan Depression

The structural evolution has been divided into three main stages.

1) Isolated fault strands, which correspond to fault development and deposition of the seismic unit 1 (Figure 11a). Rifting initiated and the fault zone developed a configuration consisting of seven main isolated fault segments. The fault strand boundaries (margins of hanging wall depocentres) were marked by transverse folds (corresponding to intra-basin topographic highs) (Figures 6 and 7).
2) Fault strand interaction and soft linkage (Figure 10b).
3) Fault strand hard linkage (Figure 10b).

The second and third stage correspond to the deposition of the seismic unit 2, during a phase of ongoing fault interaction and linkage (Figure 9), merging of the three previously isolated depocentres and subsidence as a single depocentre, after linking of the controlling fault segments to form a longer fault segment (Figure 10b). However, a minor intra-basin high still persisted in the hanging wall of F1 fault segment after the fault segments linkage, and the depocentre migration in the fault F2 segment (Figure 10).

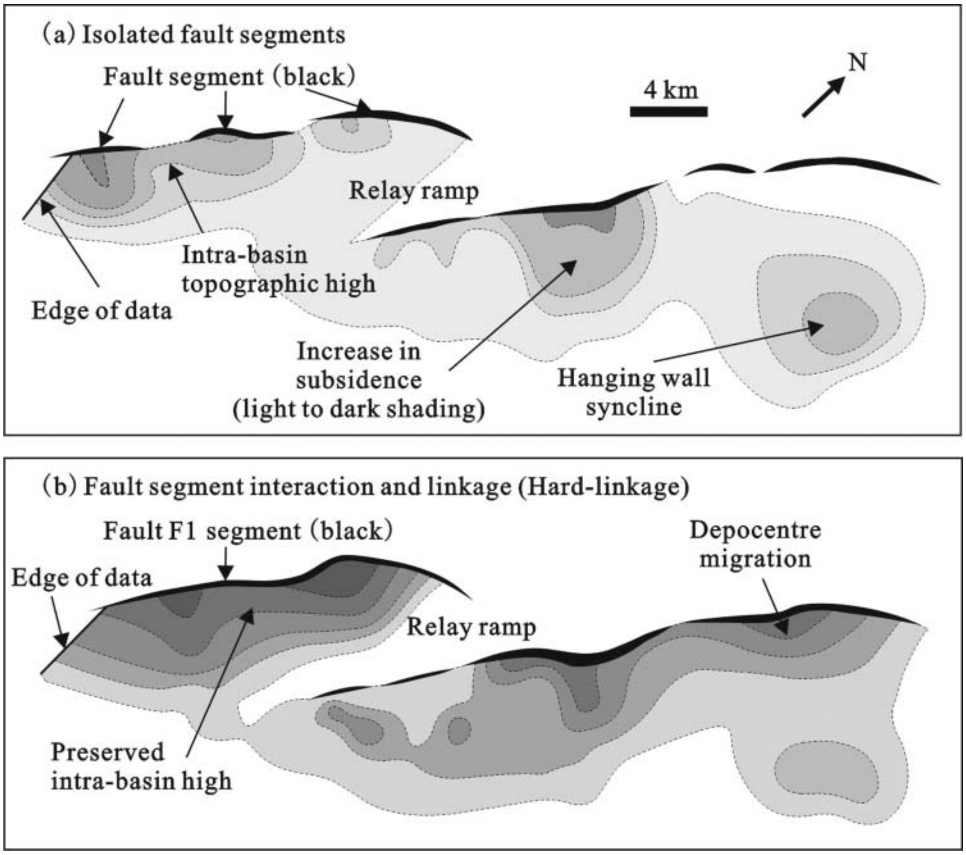

Figure 10. Three main stages of the structural evolution of the F1 and F2 (producing two fault segments separated by a relay ramp) in the Tanan Depression. The light to dark shading indicates an increasing level of subsidence. (a) Isolated fault segments; and (b) fault segments interaction and linkage (hard-linkage stage) forming a single continuous fault trace.

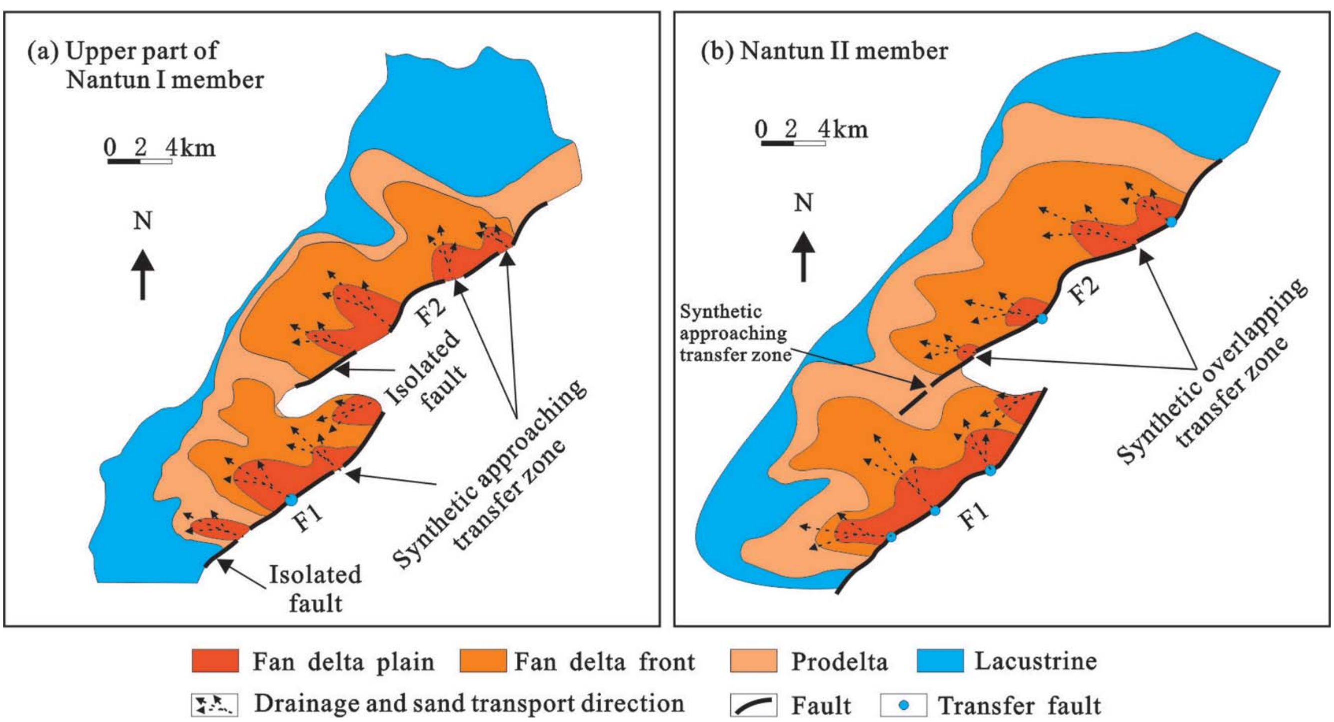

Figure 11. Relationship between structural transfer zones of different periods and sand-body distribution. Blue circle is the locus of the transfer fault. During the deposition of (a) the upper part of Nantun I member, and (b) the Nantun II member.

Controls on the location and evolution of sedimentary system in rift basins

The research indicates that paleogeomorphology dominated the direction of sediment transportation, controlled the capacity and position of sediment accommodation, and influenced the type of sedimentary facies and the spatial distribution pattern of the sediment (Fu et al., 2015; Gawthorpe & Leeder, 2000; Gawthorpe et al., 1994). Differential subsidence has led to fault displacement decreasing along the strike of fault segments, from maxima at the fault centres to minima at the fault tips or multi-minima at the segment growth point. Conversely, sediment supply may be greater within the transfer zone than at the fault tip. Studies from Lake Malawi in the East African Rift (Scholz et al., 1993) and from the Sperchios Basin in Greece (Eliet & Gawthorpe, 1995) suggest that drainage catchment areas are greatest within transfer or accommodation zones. Therefore, structural transfer zones commonly represent footwall topographic lows and hence act as a focus for major drainage systems entering into rift basins (Gawthorpe & Leeder, 2000; Jiang et al., 2016; Leeder & Gawthorpe, 1987; Morley et al., 1990; Qi, 2007; Young, Gawthorpe, & Sharp, 2000).

During the development of the Tanan Depression, the fault distribution pattern changed (Figure 8). During deposition of upper part of the Nantun I member, two synthetic approaching transfer zones and one transfer fault are formed in F1, and two synthetic approaching transfer zones are developed in F2 (Figure 11a). During deposition of the Nantun II member, F1 had formed as a through-going fault, presenting three linkage points (three transfer faults), whereas F2 comprises four fault segments, forming two synthetic overlapping transfer zones and one synthetic approaching transfer zone (Figure 11b).

The delta is situated within a transfer zone between rift-border faults; this conduit acted as a pathway for sediment that spilled over from the terrace east of the half-graben as a response to the filling of accommodation space. The transfer zones are the sediment transport pathways and can provide accommodation space for sediment discharge and deposition (Figure 11).

Discussion

Fault growth model and throw backstripping techniques

Temporal and spatial patterns of fault growth and linkage can be determined and constrained using stratigraphic information integrated with biostratigraphy and throw backstripping. Four fault growth models were illustrated by Kim and Sanderson (2005), including a constant d_{max}/L ratio model, an increasing d_{max}/L ratio model, a constant length model and a fault linkage (segment linkage) model. At present, the key question is how to reconstruct the evolution of a fault and determine the paleo-fault geometry in the different growth models. Two throw backstripping techniques were applied (Dutton & Trudgill, 2009). The original method or vertical

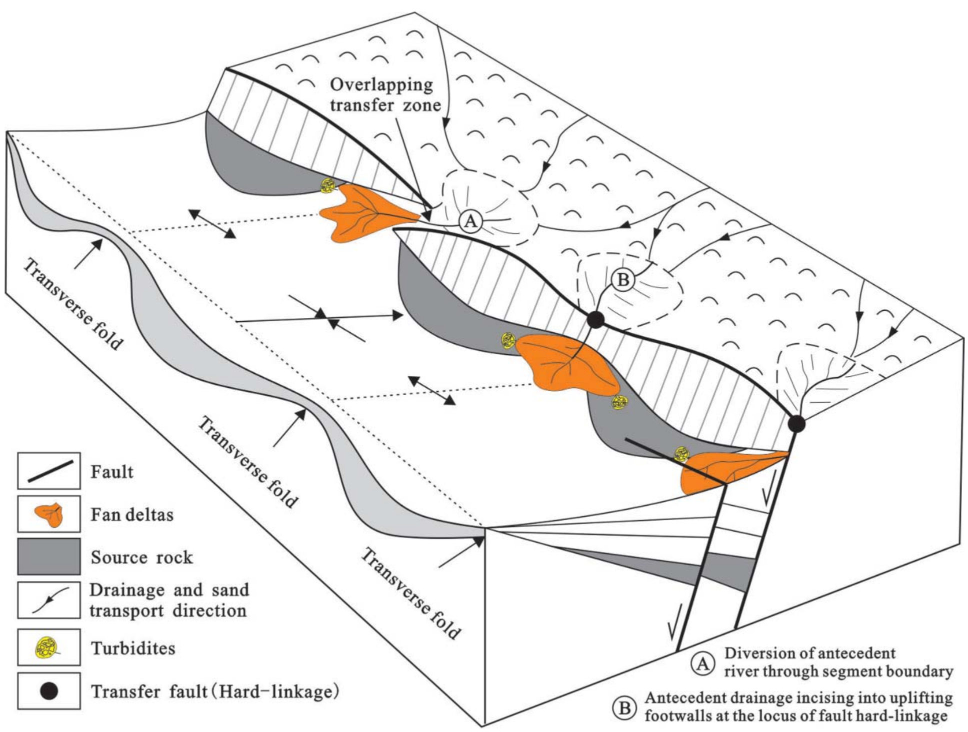

Figure 12. Tectono-sedimentary evolution of a normal fault array (continental environments). (A) Interaction and linkage stage. Consequent drainage catchments continue to develop along faceted footwall scarps and hangingwall dip-slopes and act as transverse sediment sources to developing half-graben depocentres. Location of isolated lakes is largely controlled by fault segments. (B) Hard-linkage stage. Linkage of adjacent fault segments creates major linked fault zones defining half-graben basins. Displacement on linked faults reduces topography of former intra-basin highs, allowing axial river to flow between former isolated basin segments. Note that the localisation of displacement causes increased displacement rates on active faults leading to the development of pronounced footwall topography and reversed antecedent drainage.

subtraction method (Chapman & Meneilly, 1991), in which fault length does not grow with time as throw increases (Figure 7), applies to a 'constant length model' (Walsh et al., 2002) that is widely applied for small, isolated faults (Kim & Sanderson, 2005). The second technique is the maximum throw subtraction method (T_{max}) (Rowan et al., 1998), which assumes that fault length increases with time as throw accumulates, applies to the 'constant d_{max}/L ratio model,' 'increasing d_{max}/L ratio model' and 'fault linkage (segment linkage) model.' For the fault linkage model, we can determine the isolated and hard-linkage stage of faults by the maximum throw subtraction method, but the soft-linkage stage (the characteristics of fault segments overlap) is very difficult to reconstruct in the geological history.

Variation of sedimentation patterns in the structural transfer zones

The linkage of normal fault arrays controls the early formation of rift basins and creates a series of half grabens and tilted fault blocks. Fault relay ramps are a special type of synthetic transfer zone that develop between two overlapping parallel normal faults and contain a volume of rotated rock mass with re-oriented bedding. Relay ramps are found to act as local entry points and sediment pathways for subaerial flows in some rift margin basins (Leeder & Jackson, 1993). When the footwall fault is located in the lower structural position, the relay ramps can be an entrance for mountain rivers to transport sediments into a lacustrine rift basin. In the process of deposition, the transfer zone can provide accommodation space for sediment discharge and deposition, and depocentres form at the locus of maximum throw along a fault segment (Figure 12). A noticeable feature of both footwall and hanging wall catchments and their alluvial fans is the regularity of their spacing (Gawthorpe & Leeder, 2000). The transfer zones in the footwall may feature larger-than-average drainage basins. This complex interplay between sediment supply and accommodation development will lead to different stratigraphic architectures along the length of the boundary fault zone. However, we cannot describe the detail of the control of different transfer zones on antecedent drainage and fan deltas (Figure 12).

Conclusions

This paper focuses mainly on quantitative discrimination of fault segment growth and its geological significance in the Tanan Depression, Tamtsag Basin, Mongolia. In this paper, we applied a method of quantitative restoration of fault segment growth processes that has enabled the reconstruction of the paleo-fault geometry and the syn-rift stratigraphic sequences.

1. Three methods (three diagrams) effectively discriminate the locus of fault segments linkages, including throw–distance (*T–L*) curve, fault-plane throw diagram and fault-plane depth diagram (seismic section along the fault strike).
2. The maximum throw subtraction method was used to reconstruct the evolution of faults. Application of these techniques allows *T–L* profiles to be reconstructed for various structural levels at different evolutionary stages. The F1 fault comprises four hard-linked segments and the F2 fault is divided into four soft-linked segments (F2-4 and F2-5 segments are shown by hard linkages) at the T23 structural level. The F1 fault is divided into three soft-linked segments (F1-2 and F1-3 segments are shown by hard linkages), and the F2 fault is divided into four isolated fault segments at the T23-1 structural level when the F1 and F2 are backstripped to T23 SB event.
3. Along-strike variation in fault-controlled subsidence, accommodation space and sediment supply, generate considerable strike variation in the nature and development of stratal surfaces, stacking patterns and stratal geometries. In the process of deposition, the transfer zone can provide accommodation space for sediment discharge and deposition, and depocentres are formed at the locus of maximum throw along a fault segment. This has clear implications for hydrocarbon exploration in terms of strike variation in reservoir–source geometry and continuity.
4. The results from this study have implications on the timing of normal fault evolution, in particular, to quantitatively restore paleo-fault geometry. During the deposition of the Nantun I member (seismic unit 1), seven fault segments are observed, forming seven main isochron thicks. During the deposition of the Nantun II member (seismic unit 2), three fault segments are observed, and three main isochron thicks can be observed in the hanging wall of the F1 and F2.

Acknowledgements

The authors gratefully acknowledge the Science and Technology Innovation Team in Heilongjiang Province 'fault deformation, sealing and fluid migration.' We highly appreciate the insightful comments and suggestions from Dr Yangwen Pei and another reviewer.

Disclosure statement

No potential conflict of interest was reported by the authors.

Funding

Ministry of Science and Technology of the People's Republic of China The authors gratefully acknowledge financial support from the National Natural Science Foundation of China [grant number 41602129], [grant number U1562214]; the National Science and Technology Major Project of the Ministry of Science and Technology of China [grant number 2016ZX05054-009], [grant number 2016ZX05006-005], the Major Science and Technology Project of PetroChina Company Limited [grant number 2016D-0702] and Northeast Petroleum University Excellent Research Talent Cultivation Fund-Province Innovation Reserve Talents [grant number 2017-KYYWF-0063].

ORCID

H. X. Wang http://orcid.org/0000-0002-5228-5496

References

Anders, M. H., & Schlische, R. W. (1994). Overlapping faults, intrabasin highs, and the growth of normal faults. *Journal of Geology, 102*(2), 165–179.

Athmer, W., & Luthi, S. M. (2011). The effect of relay ramps on sediment routes and deposition: A review. *Sedimentary Geology*, *242*(1–4), 1–17.

Barnett, J. A. M., Mortimer, J., Rippon, J. H., Walsh, J. J., & Watterson, J. (1987). Displacement geometry in the volume containing a single normal fault. *AAPG Bulletin, 71*(8), 925–937.

Cartwright, J. A., Mansfield, C., & Trudgill, B. (1996). The growth of normal faults by segment linkage. *Geological Society of London Special Publications, 99*(1), 163–177.

Cartwright, J. A., Trudgill, B. D., & Mansfield, C. S. (1995). Fault growth by segment linkage: An explanation for scatter in maximum displacement and trace length data from the Canyonlands grabens of SE Utah. *Journal of Structural Geology*, *17*, 1319–1326.

Chapman, T. J., & Meneilly, A. W. (1991). The displacement patterns associated with a reverse-reactivated, normal growth fault. *Geological Society London Special Publications*, *56* (1), 183–191.

Childs, C., Easton, S. J., Vendeville, B. C., Jackson, M. P. A., Lin, S. T., Walsh, J. J., & Watterson, J. (1993). Kinematic analysis of faults in a physical model of growth faulting above a viscous salt analogue. *Tectonophysics*, *228*(3–4), 313–329.

Childs, C., Manzocchi, T., Walsh, J. J., Bonson, C. G., Nicol, A., & Schöpfer, M. P. J. (2009). A geometric model of fault zone and fault rock thickness variations. *Journal of Structural Geology*, *31*(2), 117–127.

Conneally, J., Childs, C., & Walsh, J. J. (2014). Contrasting origins of breached relay zone geometries. *Journal of Structural Geology*, *58*(58), 59–68.

Coskun, B. (1997). Oil and gas fields—transfer zone relationships, Thrace Basin, NW Turkey. *Marine & Petroleum Geology*, *14*(4), 401–416.

Cowie, P. A., & Scholz, C. H. (1992). Displacement-length scaling relationship for faults: Data synthesis and discussion. *Journal of Structural Geology*, *14* (10), 1149–1156.

Dawers, N. H., & Anders, M. H. (1995). Displacement-length scaling and fault linkage. *Journal of Structural Geology*, *17*(5), 607–614.

Dawers, N. H., & Underhill, R. (2000). The role of fault interaction and linkage in controlling synrift stratigraphic sequences: Late Jurassic, Statfjord East area, northern North Sea. *AAPG Bulletin*, *84*(1), 45–64.

Dawers, N. H., Anders, M. H., & Scholz, C. H. (1993). Growth of normal faults: Displacement-length scaling. *Geology*, *21*(12), 1107–1110.

Dutton, D. M., & Trudgill, B. D. (2009). Four-dimensional analysis of the Sembo relay system, offshore Angola: Implications for fault growth in salt-detached settings. *AAPG Bulletin*, *93*(6), 763–794.

Eliet, P. P., & Gawthorpe, R. L. (1995). Drainage development and sediment supply within rifts, examples from the Sperchios Basin, central Greece. *Journal of the Geological Society*, *152*(5), 883–893.

Fossen, H. (2010). *Structural Geology* (pp. 119–185). Cambridge, UK: Cambridge University Press.

Fu, X. F., Chen, Z., Yan, B. Q., Yang, M., & Sun, Y. H. (2013). Analysis of main controlling factors for hydrocarbon accumulation in central rift zones of the Hailar-Tamtsag Basin using a fault-caprock dual control mode. *Science China Earth Sciences*, *56*(8), 1357–1370.

Fu, X. F., Sun, B., Wang, H. X., & Meng, L. D. (2015). Fault segmentation growth quantitative characterization and its application on sag hydrocarbon accumulation research. *Journal of China University of Mining & Technology*, *44*(2), 271–281 (in Chinese with English Abstract).

Fu, X. F., Xu, P., Wei, C. Z., & Lv, Y. F. (2012). Internal structure of normal fault zone and hydrocarbon migration and conservation. *Earth Science Frontiers*, *19*(6), 200–212 (in Chinese with English Abstract).

Gawthorpe, R. L., Fraser, A. J., & Collier, R. L. I. (1994). Sequence stratigraphy in active extensional basins: Implications for the interpretation of ancient basin fills. *Marine and Petroleum Geology*, *11*(6), 642–658.

Gawthorpe, R. L., & Hurst, J. M. (1993). Transfer zones in extensional basins: Their structural style and influence on drainage development and stratigraphy. *Geological Society*, *150*(6), 1137–1152.

Gawthorpe, R. L., & Leeder, M. R. (2000). Tectono-sedimentary evolution of active extensional basins. *Basin Research*, *12*(3–4), 195–218.

Graham, S. A., Hendrix, M. S., Johnson, C. L., Badamgarav, D., Badarch, G., Amory, J., … Hacker B. R. (2001). Sedimentary record and tectonic implications of Mesozoic rifting in southeast Mongolia. *Geological Society of America Bulletin, 113*(12), 1560–1579.

Gupta, A., & Scholz, C. H. (2000). A model of normal fault interaction based on observations and theory. *Journal of Structural Geology*, *22*(7), 865–879.

Hart, E. (1994). Calico Fault and Adjacent 1992 Surface Ruptures near Newberry Springs, San Bernardino County. *California Division of Mines and Geology Fault Evaluation Report*, 238. Sacramento CA: California Geological Survey CD 2002-02.

Hu, C. Y. (1982). Source bed controls hydrocarbon habitat in continental basins, East China. *Acta Petrolei Sinica, 3*(2), 9–13 (in Chinese with English Abstract).

Huang, L., Fang, S., Liu, Z. J., Zhang, J. L., Yang, B. Z., Ma, X. H., & Yang, Z. C. (2012). Characteristics of source rocks and their potential evaluation in Ta'nan sag of Tamtsag Basin, Mongolia. *Global Geology*, *31*, 148–161 (in Chinese with English Abstract).

Jackson, A. L., Gawthorpe, R. L., & Shapp, I. R. (2002). Growth and linkage of the East Tanka fault zone, Suez rift: Structural style and syn-rift stratigraphic response. *Journal of the Geological Society*, *159*(2), 175–187.

Ji, Y. L., Cao, R. C., Meng, Q. A., Zhang, G., & Qu, Y. H. (2009). Analysis of sequence structure and its controlling factors in Lower Cretaceous in Tanan Depression, Tamtsag Basin. *Acta Geological Sinica*, *83*(6), 827–835.

Jia, J. J., Liu, Z. J., Miao, C. S., Fang, S., Zhou, R. J., Meng, Q. A., Chen, Y. C., Yan, L., & Yang, D. (2014). Depositional model and evolution for a deep-water sublacustrine fan system from the syn-rift Lower Cretaceous Nantun Formation of the Tanan Depression (Tamtsag Basin, Mongolia). *Marine and Petroleum Geology*, *57*(2), 264–282.

Jiang, L., Wu, S. H., Yang, Q. H., Huang, K., Yu, B., Wang, P. … Xu Z. H. (2016). Spatial distribution and temporal evolution of sediment transport pathway of deltaic deposits in a rift basin: An example from Liaodong Bay Sub-basin, Bohai Bay, China. *Australian Journal of Earth Sciences, 64*(4), 469–483.

Kim, Y. S., & Sanderson, D. J. (2005). The relationship between displacement and length of faults: A review. *Earth-Science Reviews*, *68*(3), 317–334.

Kim, Y. S., Andrews, J. R., & Sanderson, D. J. (2000). Damage zones around strike–slip fault systems and strike–slip fault evolution, Crackington Haven, southwest England. *Geoscience Journal*, *4*(2), 53–72.

Krantz, R. W. (1988). Multiple fault sets and three-dimensional strain: Theory and application. *Journal of Structural Geology*, *10*, 225–237.

Kristensen, M. B., Childs, C. J., & Korstgård, J. A. (2008). The 3d geometry of small-scale relay zones between normal faults in soft sediments. *Journal of Structural Geology*, *30*(2), 257–272.

Leeder, M. R., & Gawthorpe, R. L. (1987). Sedimentary models for extensional tilt-block /half-graben basins. *Geological Society, London, Special Publications, 28*(1), 139–152.

Leeder, M. R., & Jackson, J. A. (1993). The interaction between normal faulting and drainage in active extensional basins, with examples from the western United States and Central Greece. *Basin Research*, *5* (2), 79–102.

Mansfield, C. S., & Cartwright, J. A. (1996). High resolution fault displacement mapping from three-dimensional seismic data: Evidence for dip-linkage during fault growth. *Journal of Structural Geology*, *18*(2–3), 249–263.

McGrath, A. (1992). *Fault propagation and growth: A study of the Triassic and Jurassic from Watchet and Kilve, North Somerset* (M.S. thesis). Royal Holloway, University of London, London. 165 p.

Meng, Q. R., Hu, J. M., Jin, J. Q., Zhang, Y., & Xu, D. F. (2003). Tectonics of the late Mesozoic wide extensional basin system in the China–Mongolia border region. *Basin Research*, *15*(3), 397–415.

Miao, C. S., Liu, Z. J., Fang, S., Chen, Y. C., Hu, F., & Wang, J. P. (2012). Characteristics of the steep-slope off-shore subaqueous fan of Nantun Formation in Ta'nan sag in Mongolia. *Earth Science, 37*(4), 771–778 (in Chinese with English Abstract).

Miao, C. S., Liu, Z. J., Fang, S., Zhang, G., Zhang, J. L., Hu, F., & Sun, X. J. (2011). Sedimentary characteristics and favorable oil-bearing facies belts analysis of near-shore subaqueous fan of Nantun formation in Tanan Depression. *Journal of China University of Petroleum*, *35*(1), 34–39.

Morley, C. K. (1995). Developments in the structural geology of rifts over the last decade and their impact on hydrocarbon exploration. *Composite Structures, 129*(1), 8–26.

Morley, C. K. (1999). Patterns of displacement along large normal faults: Implications for basin evolution and fault propagation, based on examples from east Africa. *AAPG Bulletin*, *83*(4), 613–634.

Morley, C. K. (2002). Evolution of large normal faults: Evidence from seismic reflection data. *AAPG Bulletin*, *86*(6), 961–978.

Morley, C. K., Nelson, R. A., Patton, T. L., & Mun, S. G. (1990). Transfer zone in the east African rift system and their relevance to hydrocarbon exploration in rifts. *AAPG Bulletin*, *74*(8), 1234–1253.

Morley, C. K., & Wonganan, N. (2000). Normal fault displacement characteristics, with particular reference to synthetic transfer zones, Mae Moh mine, northern Thailand. *Basin Research*, *12*(3–4), 307–327.

Muraoka, H., & Kamata, H. (1983). Displacement distribution along minor fault traces. *Journal of Structural Geology*, *5*(5), 483–495.

Opheim, J. A., & Gudmundsson, A. (1989). Formation and geometry of fractures, and related volcanism, of the Krafla fissure swarm, northeast Iceland. *Geological Society of America Bulletin*, *101*(101), 1608–1622.

Peacock, D. C. P. (1991). Displacements and segment linkage in strike-slip fault zones. *Journal of Structural Geology*, *13*(9), 1025–1035.

Peacock, D. C. P., & Sanderson, D. J. (1991). Displacements, segment linkage and relay ramps in normal fault zones. *Journal of Structural Geology*, *13*(6), 721–733.

Peacock, D. C. P., & Sanderson, D. J. (1994). Geometry and development of relay ramps in normal fault systems. *AAPG Bulletin*, *78*(2), 147–165.

Pei, Y. W., Paton, D. A., Knipe, R. J., & Wu, K. Y. (2017). Examining fault architecture and strain distribution using geospatial and geomechanical modelling: An example from the Qaidam Basin, NE Tibet. *Marine & Petroleum Geology*, *84*, 1–17.

Pollard, D. D., & Aydin, A. (1988). Progress in understanding jointing over the past century. *Geological Society of America Bulletin*, *100*, 1181–1204.

Qi, J. F. (2007). Structural transfer zones and significance for hydrocarbon accumulation in rifting basins. *Marne Origin Petroleum Geology*, *12*(4), 43–50 (in Chinese with English Abstract).

Rosendahl, B. R., Reynolds, D. J., Lorber, P. M., Burgess, C. F., McGill, J., Scott, D., Lambiase, J. J., & Derksen, S. J. (1986). Structural expressions of rifting: Lessons from Lake Tanganyika, Africa. In R. W. Renaut, I. Reid, & J. J. Tiercelin (Eds). *Sedimentation in the African Rifts* (pp. 29–43). London, UK: Geological Society London Special Publications, 25.

Rowan, M. G., Hart, B. S., Nelson, S., Flemings, P. B., & Trudgill, B. D. (1998). Three-dimensional geometry and evolution of a salt-related growth-fault array: Eugene Island 330 field, offshore Louisiana, Gulf of Mexico. *Marine and Petroleum Geology*, *15*(4), 309–328.

Schlische, R. W. (1995). Geometry and origin of fault-related folds in extensional settings. *AAPG Bulletin*, *79*(11), 1661–1678.

Schlische, R. W., Young, S. S., Ackermann, R. V., & Gupta, A. (1996). Geometry and scaling relations of a population of very small rift-related normal faults. *Geology*, *24*(8), 683–686.

Scholz, C. H., & Cowie, P. A. (1990). Determination of total strain from faulting using slip measurements. *Nature*, *346*(6287), 837–839.

Scholz, C. H., Dawers, N. H., Yu, J. Z., Anders, M. H., & Cowie, P. A. (1993). Fault growth and fault scaling laws: Preliminary results. *Journal of Geophysical Research*, *98*(B12), 21 951–921 961.

Schultz, R. A., & Fossen, H. (2002). Displacement–length scaling in three-dimensions: The importance of aspect ratio and application to deformation bands. *Journal of Structural Geology*, *24*(9), 1389–1411.

Segall, P., & Pollard, D. D. (1980). Mechanics of discontinuous faults. *Journal of Geophysical Research*, *85*(B8), 4337–4350.

Soliva, R., & Benedicto, A. (2004). A linkage criterion for segmented normal faults. *Journal of Structural Geology*, *26*(12), 2251–2267.

Traynor, J. J., & Sladen, C. (1995). Tectonic and stratigraphic evolution of the Mongolian People's Republic and its influence on hydrocarbon geology and potential. *Marine and Petroleum Geology*, *12*(1), 35–52.

Trudgill, B., & Cartwright, J. (1994). Relay ramp forms and normal-fault linkages, Canyonlands National Park, Utah. *Geological Society of America Bulletin*, *106*(9), 1143–1157.

Villemin, T., Angelier, J., & Sunwoo, C. (1995). Fractal distribution of fault length and offsets: Implications of brittle deformation evaluation—the Lorraine coal basin. In C. C. Barton & P. R. LaPointe (Eds.), *Fractal in the Earth Sciences* (pp. 205–226.). New York: Plenum.

Walsh, J. J., & Watterson, J. (1987). Distributions of cumulative displacement and seismic slip on a single normal fault surface. *Journal of Structural Geology*, *9*(8), 1039–1046.

Walsh, J. J., & Watterson, J. (1988). Analysis of the relationship between displacements and dimensions of faults. *Journal of Structural Geology*, *10*(3), 239–247.

Walsh, J. J., Nicol, A., & Childs, C. (2002). An alternative model for the growth of faults. *Journal of Structural Geology*, *24*(11), 1669–1675.

Wang, H. X., Lv, Y. F., Fu, X. F., Liu, Z. B., Meng, L. D., & Du, W. (2014). Fault quality correction and its role in the oil and gas exploration and development. *Journal of China University of Mining & Technology*, *43*(3), 461–469 (in Chinese with English Abstract).

Wang, H. X., Lv, Y. F., Fu, X. F., Sun, Y. H., Wang, H. F., & Li, P. H. (2013). Formation, evolution and reservoir-controlling mechanism of relay zone in rift basin. *Geological Science and Technology Information*, *32*(4), 102–110 (in Chinese with English Abstract).

Wang, H. Y. (2011). *Oil-gas distribution and key control factors of the central grabens in Tamuchage Basin* (PhD Thesis unpublished). Daqing China: Northeast Petroleum University (in Chinese with English Abstract).

Watterson, J. (1986). Fault dimensions, displacements and growth. *Pure and Applied Geophysics*, *124*(1–2), 365–373.

Wells, D. L., & Coppersmith, K. J. (1994). New empirical relationships among magnitude rupture length, rupture width, rupture area, and surface displacement. *Bulletin of Seismological Society of America*, *84*(4), 974–1002.

Wilkins, S. J., & Gross, M. R. (2002). Normal fault growth in layered rocks at Split Mountain, Utah: Influence of mechanical stratigraphy on dip linkage, fault restriction and fault scaling. *Journal of Structural Geology*, *24*(9), 1413–1429.

Willemse, E. J. M., Pollard, D. D., & Aydin, A. (1996). Three-dimensional analyses of slip distributions on normal fault arrays with consequences for fault scaling. *Journal of Structural Geology*, *18*(2–3), 295–309.

Young, M. J., Gawthorpe, R. L., & Sharp, I. R. (2000). Sedimentology and stratigraphy of a transfer zone coarse-grained delta, Miocene Suez rift, Egypt. *Sedimentology*, *47*(6), 1081–1104.

Young, M. J., Gawthorpe, R. L., & Sharp, I. R. (2002). Architecture and evolution of syn-rift clastic depositional systems towards the tip of a major fault segment, Suez Rift, Egypt. *Basin Research*, *14*(1), 1–23.

Zhao, X. Z., Jin, F. M., Wang, Q., Han, C. Y., & Kang, R. K. (2011). Theory of hydrocarbon accumulation in troughs within continental faulted basins and its application: A case study in Jizhong Depression and Erlian Basin. *Acta Petrolei Sinica, 32*(1), 18–24 (in Chinese with English Abstract).

Zhou, Y., Ji, Y. L., Pigott, J. D., Meng, Q. A., & Wan, L. (2014). Tectono-stratigraphy of Lower Cretaceous Tanan Sub-basin, Tamtsag Basin, Mongolia: Sequence architecture, depositional systems and controls on sediment infill. *Marine and Petroleum Geology*, *49*, 176–202.